Radboud Repository

Radboud University Nijmegen

PDF hosted at the Radboud Repository of the Radboud University Nijmegen

The following full text is a publisher's version.

For additional information about this publication click this link.
http://hdl.handle.net/2066/35453

Please be advised that this information was generated on 2017-12-06 and may be subject to change.

Astronomy & Astrophysics

Refining the fundamental plane of accreting black holes

E. Körding[1,2], H. Falcke[3,4], and S. Corbel[1]

1 AIM - Unité Mixte de Recherche CEA - CNRS - Université Paris VII - UMR 7158, CEA-Saclay, Service d'Astrophysique,
91191 Gif-sur-Yvette Cedex, France
2 School of Physics and Astronomy, University of Southampton, Hampshire SO17 1BJ, UK
e-mail: elmar@phys.soton.ac.uk
3 Radio Observatory, ASTRON, Dwingeloo, PO Box 2, 7990 AA Dwingeloo, The Netherlands
4 Dept. of Astronomy, Radboud Universiteit Nijmegen, Postbus 9010, 6500 GL Nijmegen, The Netherlands

ABSTRACT

Context. The idea of a unified description of supermassive and stellar black holes has been supported by the extension of the empirical radio/X-ray correlation from X-ray binaries to active galactic nuclei through the inclusion of a mass term. This has lead to the so-called fundamental plane of black hole activity in the black hole mass, radio and X-ray luminosity space. Two incarnations of this fundamental plane have so far been suggested using different underlying models and using two different samples of accreting black holes.

Aims. We improve the parameter estimates of the fundamental plane and estimate the scatter of the sources around the plane in both samples. This is used to look for possible constraints on the proposed theoretical models. Furthermore, we search for selection effects due to the inclusion of different classes of AGN or distance effects.

Methods. We present revised samples for both studies together with a refined statistical analysis using measured errors of the observables. This method is used to compare the two samples and infer parameters for the fundamental plane in a homogeneous way.

Results. We show that strongly sub-Eddington objects in a state equivalent to the low/hard state of X-ray binaries follow the fundamental plane very tightly; the scatter is comparable to the measurement errors. However, we find that the estimated parameters depend strongly on the assumptions made on the sources of scatter and the relative weight of the different AGN classes in the sample. Using only hard state objects, the fundamental plane is in agreement with the prediction of a simple uncooled synchrotron/jet model for the emitted radiation. Inclusion of high-state objects increases the scatter and moves the correlation closer to a disk/jet model. This is qualitatively consistent with a picture where low-state objects are largely dominated by jet emission while high-state objects have a strong contribution from an accretion disk.

Key words. X-rays: binaries – galaxies: active – radiation mechanisms: non-thermal – stars: winds, outflows – black hole physics – accretion, accretion disks

1. Introduction

Active galactic nuclei (AGN) and black hole X-ray binaries (XRBs) seem to have a similar central engine consisting of the central black hole, an accretion disk probably accompanied by a corona, and a relativistic jet (Shakura & Sunyaev 1973; Mirabel & Rodríguez 1999; Antonucci 1993). Jet and disk may form a symbiotic system (Falcke & Biermann 1995; Falcke et al. 1995) which can be scaled over several orders of magnitude in mass and accretion rate (Falcke & Biermann 1996, 1999) suggesting that a single central engine can be used to describe very different types of black holes.

While the general unification of stellar mass and supermassive black holes picture has now been established for some time, it has recently been tested on a detailed empirical level by correlations in the radio and X-ray band which have lead to the so-called fundamental plane of black hole activity (Merloni et al. 2003, hereafter MHDM; and Falcke et al. 2004, hereafter FKM). Similar unification efforts are also under way analysing and comparing the variability properties of AGN and XRBs (Uttley et al. 2002; Markowitz et al. 2003; Körding & Falcke 2004; Abramowicz et al. 2004).

To establish connections between stellar and supermassive black holes we have to consider that black hole XRBs can be found in distinct accretion states. In FKM we suggested that a number of AGN classes can be identified with corresponding XRB states and based on this proposed a power unification scheme for AGN and XRBs.

The two most prevalent XRB states are the low/hard state (LH state) and the high/soft state (HS state, see e.g., McClintock & Remillard 2006). In the LH state the radio spectrum is always consistent with coming from a steady jet (Fender 2001), which can sometimes be directly imaged (Stirling et al. 2001). Once the source enters the HS state, the radio emission seems to be quenched (Fender et al. 1999; Corbel et al. 2000). One possible scenario for the accretion flow of a LH state object is that its inner part is optically thin up to a transition radius, where the flow turns into a standard thin disk (Esin et al. 1997; Poutanen 1998). Usually, the X-ray emission of a LH state XRB is modeled using Comptonization (e.g. Sunyaev & Trümper 1979; Thorne & Price 1975), however, some models suggest that the compact jet may contribute to the X-ray emission or even dominate it (Markoff et al. 2001a; Markoff & Nowak 2004; Homan et al. 2005; Markoff et al. 2005). As the disk fades, the system may

become "jet-dominated" – meaning that the bulk of the energy output is in radiation and kinetic energy of the jet (Fender et al. 2003, FKM).

Indeed, Corbel et al. (2000, 2003) found a surprisingly tight correlation of the radio and X-ray fluxes of the black hole XRB GX 339−4 in its LH state which can be qualitatively and quantitatively well understood in the context of jet models (Markoff et al. 2003). Gallo et al. (2003) showed that this correlation does not only hold for one source but seems to be universal for all LH state XRBs. It has also been observed that, once an object enters the high state, the radio emission is quenched and it drops off the correlation (Fender et al. 1999; Tananbaum et al. 1972; Gallo et al. 2003). It has been suggested by Maccarone et al. (2003) that a similar effect can be found in AGN.

Radio/X-ray correlations have also been found for AGN, e.g., by Hardcastle & Worrall (1999) and Canosa et al. (1999). The final breakthrough came when it was shown possible to combine these correlations to a fundamental plane in the radio/X-ray/black hole mass space for XRBs and AGN (MHDM, FKM). This fundamental plane gives a tight relation between the radio and X-ray fluxes and the black hole mass, which is valid for AGN as well as XRBs. Thus, the correlation proves the similarity of the central engines of these accreting black holes.

However, there are at least two competing explanations for the fundamental plane. In the picture of FKM, the radio-through-X-ray emission for XRBs and the lowest luminosity AGN is attributed to synchrotron emission from a relativistic jet in the jet-dominated state (LH). As both components, the radio and the X-rays, originate from the same source – the jet – one can expect a tight correlation of both observables. We refer to this model as the "jet only" model. One would expect the correlation to break down once a source leaves the radiatively inefficient accretion flow state and is no longer jet-dominated. Hence, the picture should not apply for high-state objects.

On the other hand, MHDM suggested that the X-ray emission originates from the accretion flow, while the radio emission is still attributed to the relativistic jet. Both, the flow and the jet are presumed to be strongly coupled so that the radio and X-ray emission is correlated. Here we will mainly assume the accretion flow to be some variant of an advection-dominated accretion flow (ADAF, Narayan & Yi 1994; see also the convection dominated accretion flows e.g., Quataert & Gruzinov 2000) and refer to the model as "ADAF/jet" model. The ADAF solution is only one possible accretion flow model, e.g. one other possibility is presented in Haardt & Maraschi (1991). Here we will use the ADAF/jet model only as the example for possible "disk/jet" models.

In the recent past, the statistics and slopes of the radio/X-ray/mass correlations have been used to argue for and against the synchrotron/jet models (Heinz 2004, MHDM). Hence, further clarification is urgently needed. Additionally, Heinz & Merloni (2004) have used the correlation to search for constrains of the relativistic beaming. However, as we will show here, all these analyses depend strongly on the statistics of the samples, the construction of the samples, and the assumptions on the scatter of the measurements.

In this paper, we therefore investigate the problems of the parameter estimation of the fundamental plane of black hole activity. We will check the assumptions made by previous studies, and present an improved statistical analysis. We furthermore improve the samples presented by MHDM and FKM. With our refined parameter estimation method we analyze and compare both samples and investigate selection effects and the intrinsic scatter of the correlation. In this light, we discuss if the

fundamental plane can be used to constrain the underlying emission mechanism as previously suggested. We will use the intrinsic scatter to test which classes of AGN belong to the analog of the LH state XRBs.

In Sect. 2 we discuss our method of parameter estimation, the improved samples, and discuss observing frequencies. In Sect. 3 we present our results and their implications and present our conclusions in Sect. 4.

2. Parameter estimation

We are searching for the parameters of the fundamental plane for accreting black holes:

$$\log L_X = \xi_R \log L_R + \xi_M \log M + b_X, \tag{1}$$

where L_X is the X-ray luminosity in the observed band and L_R denotes radio luminosity at the observing frequency (νF_ν), M is the black hole mass, the ξ_i are the correlation coefficients, and b_X denotes the constant offset. To simplify the notation we omit the units in the logarithms. Throughout this paper all luminosities are measured in erg/s, distances in pc and masses in solar masses. In the notation we follow FKM. To derive the parameters as given in MHDM set $\xi_{RX} = 1/\xi_R$ and $\xi_{RM} = \xi_M/\xi_R$.

The predicted values for the "jet only" model are $\xi_R = 1.38$ and $\xi_M = -0.81$ (FKM), while the values for the "ADAF/jet" model are $\xi_R = 1.64$ and $\xi_M = -1.3$ (MHDM).

2.1. The samples

Here we compare the published correlations by MHDM and FKM. While both samples are used to extend the radio/X-ray correlation found in LH state XRBs, they differ in the selection of sources and which observing frequencies are used for the X-ray luminosities.

MHDM sample

The MHDM sample is a real radio/X-ray sample, i.e., it directly uses the measured radio and X-ray fluxes. It contains XRBs and nearly all types of AGN except obviously beamed sources like BL Lac objects. The sources were extracted from the literature under the condition that good mass estimates exist. To obtain a representative sample the authors selected a similar number of bright active AGN and less active AGN. The sample contains low-luminosity AGN (LLAGN), LINERs (low ionization nuclear emission region), Seyferts (type 1 and 2), FR Radio Galaxies (Fanaroff & Riley 1974) and radio loud and quiet quasars (Kellermann et al. 1989) and the quiescence flux of Sgr A*. Thus, by using this sample one averages over nearly all types of AGN, whether they belong to the LH state or not.

To avoid dealing with upper limits in the data we exclude all those limits from the MHDM sample. The overall result of the fit does not seem to change due to this, as we can reproduce the best fit values of MHDM. This sample contains some XRBs that do not follow the correlation. Cyg X−1 changes its state frequently (Gallo et al. 2003) and seems to stay always near the transition luminosity, thus, it will not trace the correlation well. GRS 1915+105 is a rather unique system that seems to stay in the "canonical" very high state most of its time (Reig et al. 2003). We therefore exclude that source as well. It is still open whether LS 5039 is a black hole or a neutron star binary. Furthermore, its radio spectrum is peculiar for a LH state object (Ribó et al. 2005). Thus, besides the original sample we will also

consider the AGN subsample of MHDM and add a subsample of the Gallo et al. (2003) XRB sample (see below). The quasar sample contains two very radio loud objects (3C273, PG 1226+023), while most quasars are radio quiet. To demonstrate the selection effects we exclude these two sources from the quasar sample when we consider subsamples of the MHDM sample.

Our sample (KFC sample)

The sample of FKM tries to include only objects in the LH state. FKM suggest to classify LLAGN, LINER, FR I Radio Galaxies and BL Lac objects as the analog classes of the LH state in XRBs. As FKM use a jet model as the basis of their suggested unification scheme, they try to compare observations at frequencies that originate from synchrotron emission (see the discussion in Sect. 2.5). They therefore extrapolate optical observations for FR I Radio Galaxies and BL Lac objects to an equivalent X-ray flux (for details see FKM). The fluxes of the BL Lac sources have been deboosted with an average Doppler factor of 7 (FKM). In the current study we further increase the number of LLAGN sources by including all sources of the Nagar et al. (2005) sample with $L_R < 10^{38}$ erg/s for which we found X-ray fluxes in the literature. We will refer to this augmented sample as the "KFC sample"[1]. The FKM LLAGN sample is based on X-ray observations of the LLAGN sample studied by Terashima & Wilson (2003). Additionally we use fluxes from the following surveys in order of preference: The Chandra v3 pipeline (Ptak & Griffiths 2003, www.xassist.org), the XMM serendipitous X-ray survey (Barcons et al. 2002), and the ROSAT HRI pointed catalog (ROSAT Scientific Team 2000). Finally, NGC 4258 fluxes were taken from Young & Wilson (2004). In the KFC sample we only consider the non-Seyfert galaxies in the Nagar et al. (2005) sample; the Seyferts of this sample will be discussed separately as, even though they are of low luminosity, they still may belong to the supermassive analog of high state XRBs, because their black hole masses are so low. For Sgr A*, we include the hard X-ray flare by Baganoff et al. (2001), as the flare may be due to jet emission (see e.g., Markoff et al. 2001b). Besides the flare we also show the result for the quiescent Sgr A* flux.

XRB sample

The sample of LH state XRBs is based on the sample of Gallo et al. (2003). To avoid problems with state transitions we only include GX 334-9, V404 Cyg, 4U 1543-47, XTE 1118+480, XTE J1550-564. For all sources we only consider the data if the source is in the LH state. We excluded GRS 1915+105 and Cyg X−1 as discussed above. For GX 334−9 (Corbel et al. 2003) we used the updated X-ray fluxes from Nowak et al. (2005).

2.2. Problems of parameter estimation

The correlation between the radio and X-ray emission has been discussed for XRBs and AGN before and it has been shown by partial correlation analysis that the correlation is indeed real (MHDM, for AGN only see Hardcastle & Worrall 1999). For a discussion of the well constrained sources Sgr A*, NGC 4258, M81 and a XRB sample see Markoff (2005). Thus, we assume that the correlation exists and only check the parameter estimation process.

---

[1] Despite other associations the reader may have with this abbreviation, it is simply based on the present authorlist.

To estimate parameters for measured data with errors in all variables, one has to use the merit function (see e.g., Press 2002, MHDM). For measurements y_i and x_{ij}, which all have uncertainties, e.g., the y_i can denote the X-ray luminosities while x_{1i} denotes the radio luminosities and x_{2j} the black hole masses, the merit function is defined as:

$$\hat{\chi}^2 = \sum_i \frac{(y_i - b - \sum_j a_j x_{ij})^2}{\sigma_{y_i}^2 + \sum_j (a_j \sigma_{x_{ij}})^2}, \qquad (2)$$

where the σ are the corresponding uncertainties, and the a_j and b are the unknown parameters. The normal χ^2 fits, which do not consider scatter in all variables, will yield asymmetric results as for them only scatter in the "y"-axis is considered. The derivative of the merit function is non-linear in the a_j and has to be solved with a numerical optimization routine. For the parameter b one can still give an analytical solution:

$$b_{\min}(\boldsymbol{a}) = \frac{\sum \omega_i \left(y_i - b_j x_{ij} \right)}{\sum \omega_i} \qquad (3)$$

with $\omega_i^{-1} = \sigma_{y_i}^2 + \sum_j \left(a_j \sigma_{x_{ij}} \right)^2$. Thus, we only have to solve a reasonably well behaved two dimensional function for which a standard numerical optimization routine can be used.

The resulting parameters depend strongly on the assumed uncertainties σ in the data. MHDM assume that these uncertainties σ are isotropic:

$$\sigma_{L_R} = \sigma_{L_X} = \sigma_M. \qquad (4)$$

Thus, they do not use measured uncertainties but set them isotropically to a value such that the reduced χ^2 is unity. This is a strong assumption and its effect has to be checked. As a first test we explore the effect of an anisotropy of the uncertainties in the mass estimation and the scatter in the luminosities, while still assuming that the uncertainties in the $L_X - L_R$ plane are isotropic:

$$\sigma_{L_R} = \sigma_{L_X} = 2\alpha\sigma_0 \qquad \text{and} \qquad \sigma_M = 2(1 - \alpha)\sigma_0. \qquad (5)$$

With these assumptions of the uncertainties, we use the merit function to derive the parameters of the original MHDM sample. The best fit values are strongly depending on the isotropy parameter α as shown in Fig. 1. An anisotropy parameter of 0.5 corresponds to an isotropic distribution of the uncertainties. For this isotropic case we can reproduce the values found by MHDM, which are also shown in the figure. $\alpha \approx 1$ corresponds to the case that the uncertainties in the luminosities dominate while for $\alpha \approx 0$ the uncertainties of the mass estimation are dominant. We observe that, for example, the parameter ξ_R can take any value between 1.4 and 3 for different α.

In case that the uncertainties only deviate slightly from the isotropic case the slope of the parameters tells us how strong these errors propagate to the final fit values. Unfortunately the slope of the parameters around $\alpha \approx 0.5$ is large. Thus, it is crucial to have a good estimate of the distribution of uncertainties. If we can improve the estimates of the uncertainties we can improve the validity of the parameter estimates. Any study based on a parameter estimate using isotropic uncertainties has to take the rather large additional uncertainties due to this assumption into account.

Besides the demonstrated effect of the anisotropy of the uncertainties of the mass estimates and the luminosity estimates, a similar effect can be found if $\sigma_{L_R} \neq \sigma_{L_X}$ We note that the best fit values do not depend on the absolute value of the combined σ but on the relative prominence of the different σ_i.
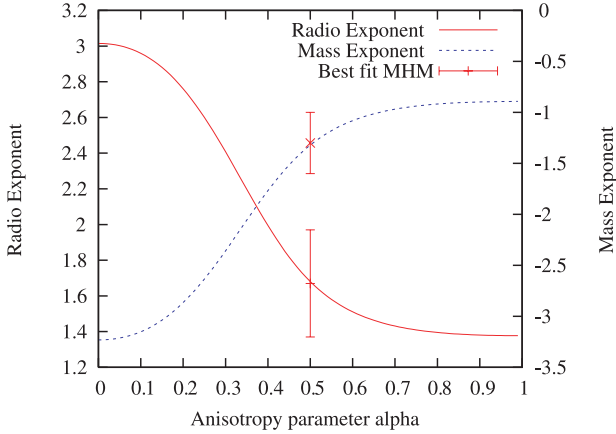
Fig. 1. The effect of anisotropic errors on the best fit parameters of the fundamental plane (Eq. (1)). The horizontal axis gives the anisotropy parameter α. A small value of α denotes that the uncertainties in the mass estimate dominate, while for large values the uncertainties of the luminosity are dominant. $\alpha = 0.5$ corresponds to isotropic errors as used by MHDM. Also shown are the best fit values of MHDM and their uncertainties. Depending on the choice of the uncertainties one can obtain values of the parameters ξ_R between 1.4 and 3 and ξ_M between –0.8 and –3.

One problem of this parameter estimation scheme is that we can not deal with coupled uncertainties. We include several measurements of the XRBs GX 339−4 and V404 Cyg so the uncertainties of the mass and distance measurements are not independent for these datapoint. We will neglect this effect for simplicity, but it may influence the estimated parameters especially for the small subsamples.

2.3. Error budget

Both luminosities depend on the measured flux and the distance, thus, the scatter in both quantities is coupled. To separate the equation into variables that have nearly independent errors, we separate the effect of the distance:

$$L_{R,X} = F_{R,X}\Xi_{R,X}D^2 \qquad (6)$$

where $F_{R,X}$ denote the measured radio and X-ray fluxes and D denotes the distance. The $\Xi_{R,X}$ are conversion factors depending on the observed band. We therefore find:

$$\log F_X = \xi_R \log F_R + \xi_M \log M + (2\xi_R - 2) \log D + b_X + \log \Xi, (7)$$

where the mathematical conversion factors are combined into Ξ. As they are just mathematical constants, they will not be discussed further.

We have seen in the previous section that the assumption of isotropic uncertainties (as used by MHDM) will effect the best fit parameters in an unknown way. To improve this situation, we estimate the errors attributed to each variable. The fluxes $F_{R,X}$ contain measurement errors and intrinsic scatter as discussed below. Besides this, the masses and distances are uncertain as well. However, as the correlation coefficient ξ_R will be around 1.4 the effect of errors in the distance estimation are less severe for the correlation than for the individual luminosities as it appears with a factor $(2\xi_R - 2)$. As the merit function requires Gaussian errors, we are always using symmetric errors in the log-log space, many of the errors below are indeed symmetric and the other parameters are only mildly asymmetric.

– Mass estimate: our XRBs LH state sample is dominated by GX 334−9 and V404 Cyg. For GX 339−4 Hynes et al. (2003) estimate a mass function of $5.8 \pm 0.5\ M_\odot$, which is therefore a lower limit for the mass of the black hole. We therefore assume a mass of $8 \pm 2.0\ M_\odot$. For V404 Cyg we use a mass of $12 \pm 2.5\ M_\odot$ (Orosz 2003 gives a range of 10–13.4 $M_\odot$). Note that there are several data points for each object. Thus, their uncertainties are coupled, which we can not take into account. The mass estimates of the other XRBs are also taken from Orosz (2003). For the AGN Merritt & Ferrarese (2001) give an absolute scatter of 0.34 dex for $M-\sigma$ relation. The mass estimate using the $M-\sigma$ relation is independent of the distance of the source (cf., Ferrarese & Ford 2005). This method is used for all galaxies except our BL Lac objects. For masses estimated with the $M-\sigma$ relation we will use the scatter of the correlation as a measure of the uncertainty for the mass estimate: 0.34 dex. We use velocity dispersions from the Hypercat catalog (Prugniel et al. 1998). For the BL Lac objects we used indirectly derived velocity dispersions from Woo & Urry (2002). Thus, these indirect measurements will have a higher uncertainty. Bettoni et al. (2001) give an uncertainty of these indirectly measured velocity dispersions σ a value of $\delta\sigma = 18\ \text{km s}^{-1}$, which yields an additional uncertainty of ≈ 0.3 dex for the mass estimate. Thus, we use an uncertainty of 0.46 dex for the mass estimate of the BL Lac objects. The indirect method to derive the velocity dispersion depends slightly on the distance. However, as we only use this method for BL Lac objects and the distances are accurate compared to 0.46 dex uncertainty, we will ignore this effect. For Sgr A*, M 81, and NGC 4258 we use direct mass measurements (see FKM), the mass uncertainties are as low as 10% (<0.05 dex).

– Distance measurement: The distance of GX 339−4 is still under debate. Shahbaz et al. (2001) and Jonker & Nelemans (2004) give a lower limit of 6 kpc, but the distance may be as high as 15 kpc (Hynes et al. 2004). We therefore adopt a distance of 8 ± 2 kpc. For V404 Cyg, we adopt the distance of 4 kpc (Jonker & Nelemans 2004). We use an uncertainty of 1 kpc, as we can not account for asymmetric uncertainties and have the issue of coupled errors. For nearby AGN we use updated distances from Maoz et al. (2005), Tonry et al. (2001). If these are not available, we use the distance estimates as given in the Tully (1988). The distance uncertainty is hard to access, as many different methods are used for which the uncertainty is sometimes not well known. We assume 40%, however, we checked that it does not change the result if one assumes less scatter. For AGN with distances derived from the Hubble law, we use an error estimate based on the peculiar velocities in the Hubble flow and the uncertainties of the Hubble constant (we assume $H_0 = 72\ \text{km s}^{-1}\ \text{Mpc}^{-1}$ Spergel et al. 2003, 5% uncertainty, $\Omega_\Lambda = 0.7$ and $\Omega_M = 0.3$). Hawkins et al. (2003) give a peculiar velocity of $506\ \text{km s}^{-1}$ which corresponds to 6.7 Mpc. Thus, for most sources the distance uncertainty is mainly due to the uncertainty in the Hubble flow. For the MHDM sample, we use the distances as provided by MHDM and assume a constant uncertainty of 40% in the distance estimation to avoid that we overestimate the intrinsic scatter, see below. Here, we also checked that this assumption is not critical. For most sources MHDM derive the distance from the Hubble law, so that the uncertainty is mainly due to the Hubble constant.

– Flux measurements: for all but the faintest objects are the fluxes very well constrained. Errors for radio and

optical/X-ray fluxes are usually less than 10%. Systematic errors, e.g., due to the extrapolation of the different observed energy bands to our used X-ray band (0.5–10 keV), will also be of a similar magnitude. Thus, as these errors are small compared with the scatter due to the mass measurements, we do not introduce significant changes by assuming that these errors are isotropic. Due to this assumption, it is possible to unify these flux errors with the intrinsic errors of the source.

– Intrinsic errors: besides the measurement errors above, there are several sources of intrinsic scatter of often unknown magnitude:
  – Non-simultaneous observations of the AGN: the radio and X-ray observations are non-simultaneous, there is often more than a year between the different observations. All accreting black holes (AGN and XRBs) are highly variable. Thus, already this effect can lead to a deviation by more than an order of magnitude. The orientation of this uncertainty is likely to be isotropic.
  – Beaming: in most models at least the radio emission is attributed to the relativistic jet and will thus be relativistically beamed. In case that the X-rays originate from the disk/corona they will not be beamed and the deviations from the correlation will be enormous. For jet models, the X-ray emission may be beamed like the radio emission or have a different beaming patters (e.g., a velocity structure in the jet Chiaberge et al. 2000; Trussoni et al. 2003). The asymmetry of this effect depends on the exact model, so we can only assume isotropy.
  – Source peculiarities: the surrounding environment of the black hole will play a role on the exact emission properties (e.g., there might be compact hotspots). There may also be an obscuring torus or other obstacles for the emission. This can result in strong X-ray absorption or the radio emission may also be absorbed. All models, however, only consider the nuclear emission.
  – Spectral energy distribution (SED): depending on the real emission model, it may be that we are not observing the same emission type in the X-rays for the different objects. For jet models the effect of radiative cooling and the synchrotron cut-off have to be mentioned (see Sect. 2.5). For disk models a similar effect may be due to the relative strength of the disk component, the jet component as observed in the resolved X-ray jets, and the Comptonization component. The X-rays in XRBs may not originate from the same process as those in AGN due to the mass scaling by whatever theory is used.

The total intrinsic scatter will be derived from the scatter of the correlation. We will see below that the intrinsic scatter is surprisingly small considering this long list of possible errors.

For the two last sources of scatter, the flux measurements and the intrinsic errors, we do not have an exact knowledge of their magnitude and their asymmetry. We will therefore assume that they are isotropic in the $\log F_X - \log F_R$ plane and parameterize their combined magnitude as σ_{Int}. This parameter σ_{Int} will be chosen, such that the reduced merit function is unity. With this choice we assume the error distribution just described; this will therefore affect the final fit values. If one distributes the excess variance in a different manner one will find slightly different best fit parameters. However, as we know several effects that introduce uncertainties in the radio and X-ray fluxes and the the excess variance in these variables is surprisingly low, it is
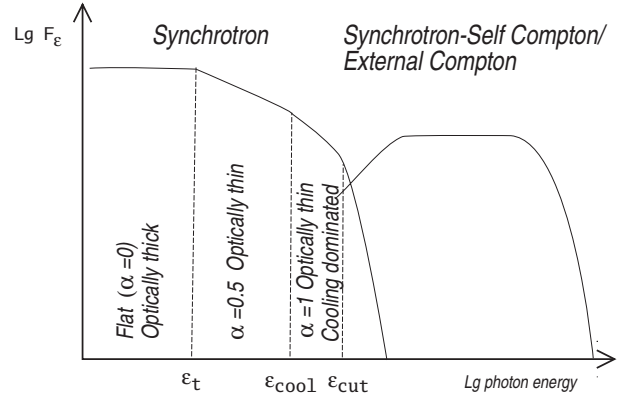

Fig. 2. Sketch of the SED of a relativistic jet as for example observed in BL Lac objects. At lower photon energies synchrotron emission is dominant while the high energy spectrum is usually explained by inverse Compton processes. See text for details.

sensible to include the excess variance only in the radio and X-ray fluxes.

2.4. The parameter σ_{Int}

In Sect. 2.3 we present our assumptions on the uncertainties of the measured variables. In case that these assumptions are exact, e.g., the magnitude of the uncertainties and that they are Gaussian distributed, the fitted parameter σ_{Int} will describe the real intrinsic scatter of the sources. This value could then be used to constrain the different contributions like the effect of beaming. However, if we overestimate the uncertainties in the flux, distance, and mass estimation the derived σ_{Int} will be too small. Similarly, an underestimation will lead to an overestimation of the intrinsic scatter.

Our method can not treat coupled uncertainties correctly. For XRBs we include several data points for each source, but there is only one mass and distance estimates for that source. Thus, as we have to assume that our uncertainties are independent, we overestimate the measurement errors. Thus, the inferred σ_{Int} for XRBs alone is zero. This means that the deviations of the data points from the optimal correlation is within the measurement uncertainties. On the other hand, for the AGN samples the uncertainties are independent. Every source is included only once in the sample. Here, σ_{Int} should be a good measure for the intrinsic scatter.

2.5. Origin of X-ray emission in the jet model

The spectrum of a relativistic jet can be directly observed in BL Lac objects, as relativistic boosting increases the relative prominence of the jet component compared to the disk (Blandford & Rees 1978). An idealized spectrum of a jet, i.e., the "Camel's back", is shown in Fig. 2 in flux (F_ϵ) representation. Such a jet component exists at least in every AGN with a detectable jet, most likely in all AGN. The relative prominence of this component in respect to disk and corona emission will vary. Furthermore, the exact shape of the SED depends also on the inclination angle, the Lorentz factor of the jet and peculiarities of the source.

The spectrum of a conical jet is flat (in F_ν representation) due to optically thick synchrotron emission up to the turnover frequency ϵ_t. This is followed by the optically thin power law component with a typical energy index α ($F_\epsilon \sim \epsilon^{-\alpha}$) of around

$\alpha = 0.5$. This emission comes from the innermost region of the radiating jet. The power law continues up to the energy where radiative cooling plays a role (ϵ_{cool}); here the power law may steepen to $\alpha \approx 1$. Finally the synchrotron emission cuts off at (ϵ_{cut}), due to the acceleration mechanism creating the radiating particles. At photon energies above the synchrotron cut-off, synchrotron-self Compton emission and external Compton emission are visible. As the jet is relativistically boosted, the total observed power in these two humps depend on the jet Lorentz factor and the inclination of the source. The relative prominence of the synchrotron and the inverse-Compton emission depends on these two parameters as well.

The photon energy where the synchrotron emission cuts off, seems to depend on the total power of the accreting system, see e.g., the blazar sequence (Fossati et al. 1998; Ghisellini et al. 2002). For low power systems, like high-peaked BL Lac objects (see the previous references), the cut-off energy can be above or around the standard X-ray band of 0.5–10 keV, while for strongly accreting systems, e.g., flat spectrum radio quasars, this cut-off can be as low as 0.1 eV. Thus, we can expect that only the X-rays of low power systems actually originate from synchrotron emission.

Radiative cooling in the X-rays, as for example discussed by Heinz (2004), may play a role in some sources of low to intermediate accretion rates. Its main effect will be that the measured X-ray flux will be reduced to what one would expect from a simple uncooled jet. However, the X-ray reduction due to cooling is far less severe than the synchrotron cut-off. The effect of cooling will increase the observed intrinsic scatter as we are exploring only the simplest jet model: the uncooled jet. For most AGN besides the LLAGN in the MHDM sample this synchrotron cut-off will be below the X-ray band. The X-ray emission in these sources will not be due to synchrotron emission. It will either originate from inverse-Compton processes in the jet or from the disk/corona.

The cut-off energy (ϵ_{cut}) of LLAGN sources in the KFC sample will for most sources be above the ROSAT and Chandra bands. The radio luminosities of the LLAGN are in the range of 10^{36-38} erg/s. If one extrapolates Fig. 7 of Fossati et al. (1998) to these energies, one can expect a cut-off above 10^{19-20} Hz or 40–400 keV. For BL Lac objects and FR-I RGs, the KFC sample extrapolates optical fluxes to an equivalent X-ray flux. This treatment avoids the effect of the synchrotron cut-off also for these sources. The "jet only" model should therefore be applicable to the KFC sample.

2.6. Origin of the X-ray emission in the MHDM sample

The X-ray emission of many sources in the MHDM sample is very likely not due to synchrotron emission, due to the synchrotron cut-off. For example, for radio loud quasars, the synchrotron cut-off is far below the X-ray regime (see e.g., Tavecchio et al. 2002). Only the X-ray emission from the LLAGN may originate from synchrotron emission. Thus, the "jet-only" model is not applicable to the MHDM sample, and can therefore not be constrained using the MHDM sample.

The AGN sample of MHDM contains radio loud objects (e.g., Cyg A, 3C273, etc.). The X-ray spectral index of radio loud Quasars (RLQ) and those of radio quiet Quasars (RQQs) seems to be different: $\Gamma_{RLQ} \approx 1.63 \pm 0.02$ compared to $\Gamma_{RQQ} \approx 1.89 \pm 0.11$. Furthermore, RLQ show very weak or no reflection components and the strength of the soft excess seems to be anti-correlated with the radio-loudness. These effects are usually explained by a relativistic jet component in the RLQ case (see e.g., Reeves & Turner 2000; Piconcelli et al. 2005).

On the other hand, there are several detected "resolved" X-ray jets in AGN. For the source 3C273, which is included in the MHDM sample, see Marshall et al. (2001). Marshall et al. (2005) and Sambruna et al. (2004) find in more than 50% of the observed radio loud sources resolved X-ray jets. The authors suggest that all bright radio jets may have X-ray counterparts. The X-ray emission from the AGN jets is usually explained by non-thermal processes (synchrotron, inverse-Compton, synchrotron-self-Compton), which process dominates seems to vary from source to source. For a discussion see Harris & Krawczynski (2002). As the jet is visible, it most likely contributes at least at some level to the core X-ray flux. Furthermore, many of the MHDM fluxes are derived from ASCA or GINGA data. In that case, the Chandra resolved X-ray jet will be observed as a point source. Note that the X-ray jets in AGN are often dominated by emission from knots, unlike what is expected for LH state XRBs as modeled by Markoff et al. (2001a). From the statistical studies and the direct observation of X-ray jets, we conclude that *at least some radio loud AGN in the MHDM sample have an X-ray component originating from the jet.*

Besides jet components, other features can contaminate the X-ray fluxes, especially for non-Chandra data. The flux may consist of several components originating from different physical processes, including the disk described by any model, the corona, the reflection component, warm gas and the jet (at least in radio loud objects).

2.7. Uncertainties of the estimated parameters

Given the data points and their estimated uncertainties we can derive the optimal fit parameters from Eq. (2). The merit function $\hat{\chi}^2$ can be used similarly to the usual χ^2 to estimate the confidence region of the parameters. The 1σ confidence region should be given by $\Delta\hat{\chi}^2 \approx 2.3$ as we have 2 degrees of freedom in our model besides the offset b_X. As problems may arise due to the use of the nonlinear merit function or the unknown distribution function of the errors, we checked that this confidence region is in agreement with the confidence region derived by a Monte Carlo simulation and the Bootstrap method (see below).

In the Monte-Carlo simulation, the errors of the parameters are estimated by creating a large number (5000) of artificial datasets that have similar statistical properties compared to the measured dataset. For each of the artificial datasets, we estimate the best-fit parameters using the same method as for the original dataset. From these fitted parameters, we derive the confidence region and the $\Delta\hat{\chi}^2$ corresponding to the 1, 2 and 3σ confidence regions. To create the artificial data, we consider each population of sources of our measured dataset individually and measure their scatter and position in the $\log L_R$–$\log L_X$ plane. In the artificial dataset, we distribute the sources uniformly over their radio luminosities. The artificial dataset will therefore also contain simulated objects of all considered types. We assume that the scatter compared to the real correlation is Gaussian. As seen in Fig. 3 this seems to be roughly the case. We also introduce flux limits in the simulation to access the effects of the distance selection effect.

The bootstrap method functions as follows. From a set of N measured sources, we draw N at random with replacement, thus, creating an artificial dataset. This dataset contains some of the sources more than once, while others are omitted. The parameters of the fundamental plane will be estimated for this sample in the same way as for the original dataset. These simulated
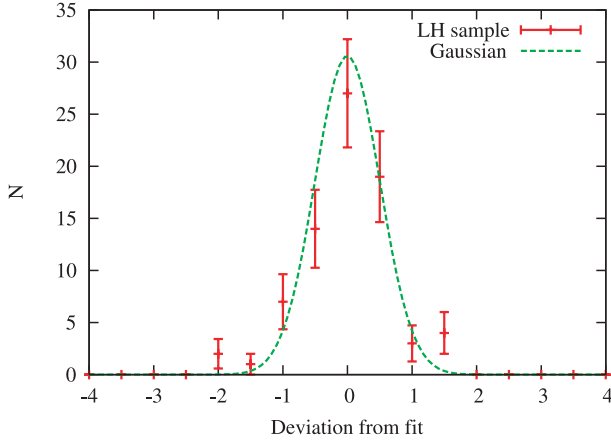
Fig. 3. Histogram of the scatter in the full KFC sample. The scatter can be well approximated by a Gaussian with the standard-deviation $\sigma = 0.50$.

parameters should be distributed around the original best fit values as the measured parameters are distributed around the real parameters (Press 2002). The benefit of this method is that it does not require prior knowledge of the distribution function from which the original dataset was drawn.

2.8. Different parameter estimators

Up to now we have only discussed the parameter estimation using the merit function (Eq. (2)). This method minimizes the average distance of the data-points from the plane weighted with the measured uncertainties. Other possible methods used in astronomy include the ordinary least squares estimation or Maximum Likelihood methods (see e.g., D'Agostini 2005). Even though Maximum Likelihood estimators find the most probable parameters of a model, the method is often biased towards lower fit parameters. To find the optimal fitting method for our problem, we compare the different fitting methods using a Monte Carlo simulation. We create several artificial samples with our Monte Carlo simulation and compare the results of the different estimators with the parameters used to create the sample. We set the intrinsic scatter of our artificial XRB and LLAGN sample to 0.2 and for BL Lac and FR-I RGs to 0.8, which is roughly double of what is found in our sample. The resulting intrinsic scatter of the simulated sample is $\sigma_{int} = 0.65$. For each parameter estimator consider two cases: First, we only use the average intrinsic scatter (0.65) to estimate the parameters, and second, we use the exact probability distribution used to create each individual data-point.

For each estimator we simulated 100 different datasets and give the average estimated parameters and the standard deviation in Table 1. While the merit function seems to be a fairly robust method, the maximum likelihood estimator is biased towards smaller fit values. Thus, we will estimate our parameters with the method using the merit function described in Sect. 2.

3. Results

Our fitting algorithm is only robust if our sources are normally distributed around the fundamental plane. As a first test we show a histogram of the scatter of the KFC sample around the best fit to the fundamental plane in Fig. 3. The deviations are roughly normally distributed with $\sigma \approx 0.5$. Thus, the developed analysis method can be utilized.

We fitted the KFC sample with the fundamental plane described in Eq. (7). The parameter estimation method is described in Sect. 2. We find as best fit values

$$\xi_R = 1.41^{+0.14}_{-0.12} \quad \xi_M = -0.87^{+0.15}_{-0.17} \quad b_X = -5.01^{+3.35}_{-3.9}. \tag{8}$$

The confidence region of the two relevant parameters and the fit is shown in the top panel of Fig. 4. The given uncertainties are derived from the $\Delta\hat{\chi}^2$ map. The intrinsic scatter in the fundamental plane is for this sample $\sigma_{int} = 0.38 \pm 0.06$. The uncertainty of σ_{int} has been derived by bootstrapping the measured sample.

The results of the KFC sample and the MHDM sample and their subsamples is presented in Table 2. The errors given in this table are derived using the Bootstrap method. As the errorbars for the KFC sample are nearly identical for both methods, we present only the bootstrapped errorbars for the different subsamples. This error estimation is less dependent on the assumption of normal distributed scatter. As the uncertainties are not strongly anisotropic, we give a symmetric uncertainty to avoid problems with anisotropic errors. We note that the different fit values do not coincide within the errors for both samples due to the different source populations included in the sample.

The subsample of the KFC sample containing no FR-I radio galaxies has a larger radio coefficient ($\xi_R = 1.64 \pm 0.13$) and a smaller mass coefficient ($\xi_M = -1.08 \pm 0.14$) than the full sample. On the other hand, the subsample without BL Lac objects deviates in the other direction ($\xi_R = 1.25 \pm 0.1$ and $\xi_M = -0.74 \pm 0.12$). This difference arises, because FR-I radio galaxies are fainter in the optical and X-rays than the deboosted BL Lac objects (Chiaberge et al. 2000). The difference in the optical/X-ray luminosity can be explained by a velocity structure in the jet. As we include a similar number of BL Lac objects and FR-I radio galaxies in the full sample, these effects will partly average out. However, the final value for the parameters will depend on the total weight each AGN class has in the total sample.

The KFC subsample containing only XRBS, Sgr A* and LLAGN has similar best fit values as the subsample containing no FR-I RGs. Its correlation coefficient, $\xi_R = 1.59 \pm 0.21$, is larger than the one found for the full sample. This is partly due to the fact that the intrinsic scatter of this subsample is extremely low: $\sigma_{int} = 0.12$. Thus, the errors of the mass estimation dominate (0.34 dex) the overall error budget and one gets larger fit values as shown in Fig. 1. If one adds Seyferts and Transition objects, which may correspond to the high state, the correlation coefficient gets even larger. However, all KFC subsamples seem to be roughly in agreement with $\xi_R \approx 1.4$ and $\xi_M \approx -0.8$. This radio coefficient is in agreement with the radio/X-ray correlation for GX 339−4, which has $\xi_R \approx 1.4$ (Corbel et al. 2003).

If one uses the quiescent flux of Sgr A* instead of the flare by Baganoff et al. (2001) in the KFC sample the best fit values for ξ_R increase. The subsample containing only XRBs, the quiescent Sgr A* and LLAGN yields $\xi_R = 1.97$ and $\xi_M \approx -1.41$. Interestingly, the latter subsample has an intrinsic scatter of zero, i.e., the scatter of the correlation is in agreement with the assumed measurement errors. However, the inferred fit for ξ_R is no longer in agreement with the value found for XRBs only ($\xi_R = 1.4$). The quiescent X-ray emission from Sgr A* is an extended (Baganoff et al. 2003), while this is not the case for cores of the XRBs or AGN. Thus, it is not surprising that the fit values change.

For the previous fits we have used the same intrinsic scatter σ_{int} for all our objects. However, we have seen that XRBs and LLAGN can be fitted with significantly less excess scatter than the full sample. Thus, we can fix the intrinsic scatter of XRBs

Table 1. Performance of the different parameter estimators. The given uncertainties is the standard deviation of the fit parameters obtained from different artificial datasets.

Estimator	ξ_R	ξ_M	b_X
Assumed parameters	1.40	−0.85	−4.9
Merit function	1.42 ± 0.13	−0.87 ± 0.16	−5.4 ± 3.6
Merit function with exact knowledge of scatter	1.40 ± 0.08	−0.85 ± 0.09	−4.8 ± 2.3
Merit function with isotropic uncertainties	1.54 ± 0.16	−1.03 ± 0.19	−8.5 ± 4.4
Maximum likelihood	1.10 ± 0.08	−0.47 ± 0.09	3.5 ± 2.1
Maximum likelihood with exact knowledge of scatter	1.25 ± 0.06	−0.68 ± 0.07	−0.51 ± 1.68
Ordinary least squares	1.09 ± 0.08	−0.46 ± 0.09	4.0 ± 2.3
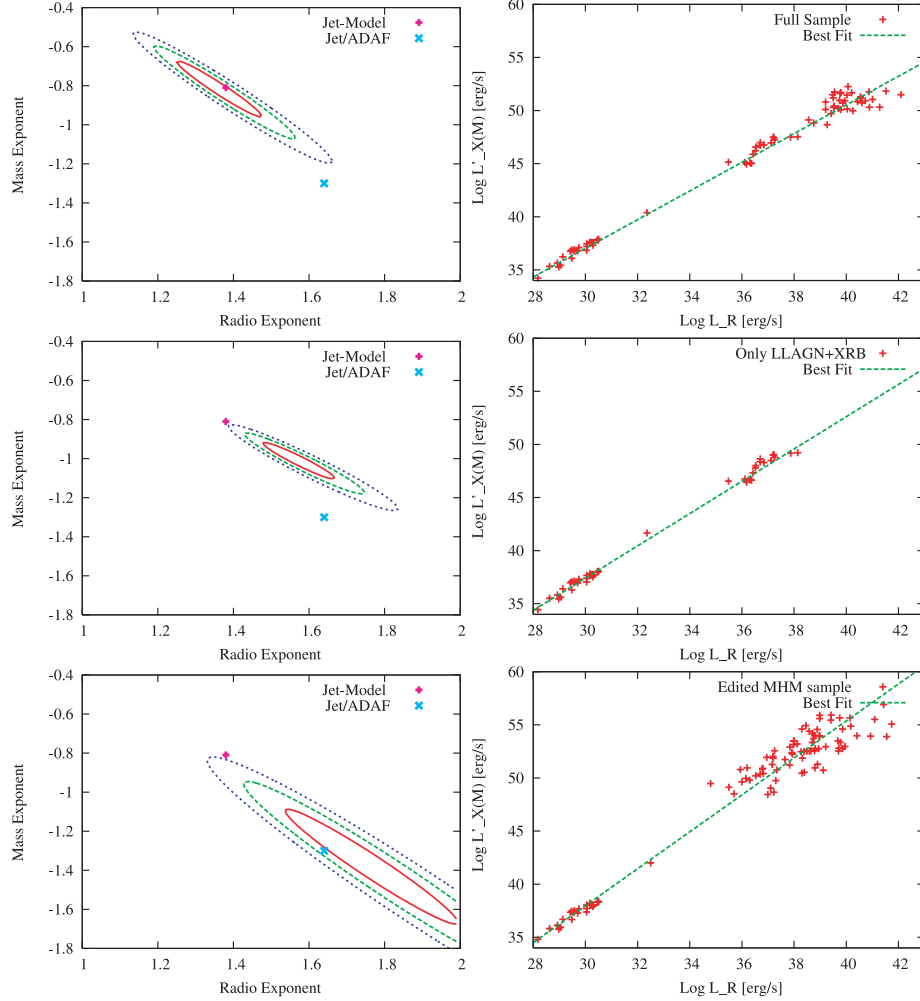
Fig. 4. On the left side we show the χ^2 map with one (solid line), two (dashed) and three sigma (dotted) levels together with the predictions of the "jet only" model and the ADAF/jet model. The right side shows the best fit and the AGN and XRB sample. The three rows show the different samples, *from Top to bottom*: KFC sample, Only XRBS and LLAGN of the KFC sample, and the edited MHDM sample.

and LLAGN to 0.1 dex and fit only the scatter in the BL Lac and FR-I RGs. Now, we find $\xi_R = 1.61 \pm 0.11$ and $\xi_M = −1.08$ which is similar to the result found for XRBs, Sgr A* and LLAGN only. The intrinsic scatter found for FR-I RGs and BL Lac objects is 0.55 dex. The statistical weight for these two classes is therefore significantly less than that of the LLAGN and XRBs. It is therefore not surprising that we find similar fit values: the fitting method puts only very a low weight on the additional sources. To observe selection effects it is therefore sensible to use a constant intrinsic scatter for all sources.

For the full edited MHDM sample, we find $\xi_R \approx 1.74^{+0.23}_{-0.19}$ and $\xi_M \approx −1.35^{+0.24}_{-0.30}$. As for the KFC sample, we also find a

selection effect for the MHDM sample. The MHDM subsample containing no Seyfert objects yields as best fit parameters $\xi_R \approx 2.12$ and $\xi_M \approx −1.75$, while the one containing no Quasars gives $\xi_R \approx 1.55$ and $\xi_M \approx −1.15$. This effect can be explained by the fact that the quasars are more radio quiet than the other AGN in the sample. We note that the formal fits of ξ_R for most subsamples tend to be significantly higher than the value found by Corbel et al. (2003) of $\xi_R = 1.4$ for XRBs. Overall, we find the choice of the sample strongly influences the final fit value in both considered samples (MHDM and KFC). This is not necessarily worrisome, as one does expect somewhat different results for different black hole states.

Table 2. Best fit results for the KFC sample and the original and edited MHDM sample. Besides the full sample we also give the parameters for the subsamples containing only a limited set of AGN classes. Note that LINER sources classified by MHDM are not limited to LLAGN. The LH XRB sample is defined in Sect. 2.1. The column N denotes the number of sources in the sample.

|	ξ_R	ξ_M	b_X	σ_{int}	$\xi_m|\xi r = 1.4$	$\sigma_{int}|\xi r = 1.4$	N
KFC sample							
Full sample (XRB, Sgr A*, LLAGN, FR-I, BL Lac)	1.41 ± 0.11	-0.87 ± 0.14	-5.01 ± 3.20	0.38	-0.86 ± 0.02	0.38	77
Full sample + Seyferts & Transition obj.	1.48 ± 0.13	-0.95 ± 0.16	-6.89 ± 3.83	0.44	-0.86 ± 0.02	0.44	100
XRB, Sgr A*, LLAGN, FR-I	1.25 ± 0.10	-0.74 ± 0.12	-0.46 ± 2.93	0.28	-0.91 ± 0.02	0.30	58
XRB, Sgr A*, LLAGN, BL Lac,	1.64 ± 0.13	-1.08 ± 0.14	-11.67 ± 3.59	0.18	-0.81 ± 0.02	0.23	62
XRB, Sgr A*, LLAGN	1.59 ± 0.21	-1.02 ± 0.21	-10.15 ± 6.17	0.12	-0.84 ± 0.02	0.15	43
XRB, Sgr A*, LLAGN, Seyfert & Transition	1.86 ± 0.35	-1.33 ± 0.36	-17.98 ± 9.92	0.35	-0.85 ± 0.02	0.39	66
Sgr A*, LLAGN, FR-I, BL Lac	1.70 ± 1.17	-2.17 ± 4.09	-5.21 ± 12.08	0.45	-1.15 ± 0.38	0.46	52
Full sample with quiescent Sgr A*	1.52 ± 0.14	-1.00 ± 0.18	-8.15 ± 4.11	0.39	-0.85 ± 0.02	0.40	77
XRB, quiescent Sgr A*, LLAGN	1.97 ± 0.11	-1.41 ± 0.10	-21.05 ± 3.05	0.00	-0.86 ± 0.02	0.23	43
Original MHDM sample	1.45 ± 0.17	-0.99 ± 0.22	-5.98 ± 5.02	0.72	-0.93 ± 0.03	0.73	116
MHDM sample with LH XRBs							
Full sample (XRB, Sgr A*, LINER, Quasar, Seyfert)	1.74 ± 0.20	-1.35 ± 0.27	-14.23 ± 5.75	0.65	-0.92 ± 0.03	0.68	103
XRB, Sgr A*, LINER, Seyfert	1.55 ± 0.19	-1.15 ± 0.24	-8.93 ± 5.37	0.64	-0.96 ± 0.03	0.64	92
XRB, Sgr A*, LINER, Quasar	2.12 ± 0.31	-1.75 ± 0.38	-25.20 ± 8.81	0.51	-0.90 ± 0.04	0.62	57
XRB, Sgr A*, Quasar, Seyfert	1.79 ± 0.28	-1.39 ± 0.37	-15.68 ± 7.87	0.63	-0.88 ± 0.03	0.65	82
XRB, Sgr A*, LINER	1.59 ± 0.35	-1.19 ± 0.40	-10.11 ± 10.13	0.50	-1.54 ± 0.21	0.71	46
XRB, Sgr A*, Quasar	2.03 ± 0.28	-1.55 ± 0.36	-22.76 ± 7.86	0.14	-0.74 ± 0.04	0.32	37
Sgr A*, LINER, Quasar, Seyfert	1.65 ± 0.26	-1.72 ± 0.50	-8.02 ± 8.06	0.74	-1.41 ± 0.22	0.76	78
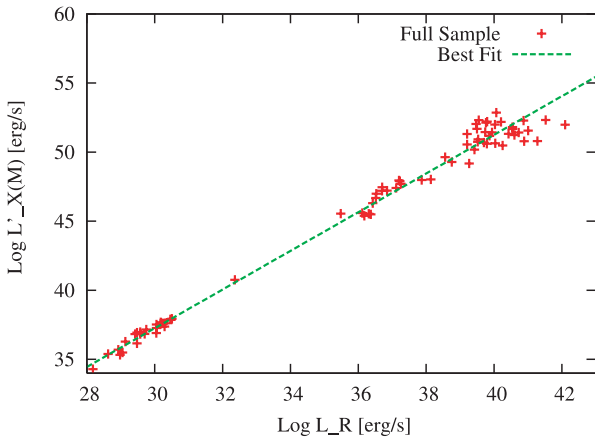
Fig. 5. Best fit for the full KFC sample if one fixes ξ_R to 1.4, which is the value found for XRBs. Only the mass scaling parameter is fitted. One finds: $\xi_M = -0.86 \pm 0.02$ and $b_X = -4.9$. The intrinsic scatter increases by less than 0.01 compared to the fit in both parameters ($\sigma_{int} = 0.38$).

The correlation index ξ_R for XRBs only is better constrained than in the case we are considering here, as one does not have to consider the mass scaling in that case. For XRBs only one finds $\xi_R \approx 1.4$ (Corbel et al. 2003; Gallo et al. 2003). If we use this prior knowledge to fix the correlation index ξ_R to 1.4 and only fit the mass scaling parameter ξ_M to our full KFC sample, we find $\xi_M = -0.86 \pm 0.02$ (see Table 2). This fit is shown in Fig. 5. The fit is not significantly worse than the original fit in both parameters, as the intrinsic scatter increases by less than 0.01 ($\sigma_{int} = 0.38$). Interestingly, the best fit value for the

subsample of LLAGN, that had a higher correlation ($\xi_R = 1.59$) yields with the prior knowledge $\xi_M = -0.84 \pm 0.02$, in agreement with the value found for the full sample. For the MHDM sample, we find $\xi_M = -0.92 \pm 0.04$. As the correlation index ξ_R is well constrained for XRBs, fixing $\xi_R = 1.4$ will likely yield the best estimates for the parameters of the fundamental plane.

Besides checking the effect of anisotropic errors we also explore the effect that the uncertainties are not normally distributed but exponentially. In that case, one does not minimize the square of the deviations divided by the uncertainty but the absolute value. This "robust" estimation (Press 2002) yield $\xi_R = 1.39$ and $\xi_M = -0.84$. For the edited MHDM sample we find $\xi_R = 1.63$ and $\xi_M = -1.14$. Thus, the change of the distribution of the uncertainties does not significantly change the best fits.

In Table 2, we also show the intrinsic scatter measured for the different datasets. If we drop our assumption that the intrinsic scatter is the same for AGN and XRBs, e.g. if σ_{int} is smaller for XRBs than for AGN, then the correlation coefficient ξ_R will rise slightly.

3.1. The distance selection effect

Our sample of AGN and XRBs is a random sample of well studied objects and not a complete distance limited sample. Thus, one can fear that the fundamental plane is a spurious correlation created by distances selection effects. It has been shown with partial correlation analysis by MHDM that the fundamental plane is real and not spurious. This problem has been discussed in detail by Merloni et al. (2006), where the authors show further statistical and observational evidence that the fundamental plane

Table 3. Effect of the observing flux limits on correlated data: most radio fluxes in our sample are obtained with the VLA, which can detect 0.1 mJy within a 10 min snapshot. Chandra can go as deep as 10^{-14} erg/s/cm^2 in a 1000 s observation.

Radio limit [mJy]	X-ray limit [erg/s/cm^2]	ξ_R	ξ_M	b_X
no limit	no limit	1.40 ± 0.11	-0.86 ± 0.15	-4.84 ± 3.2
0.5	10^{-13}	1.37 ± 0.11	-0.80 ± 0.15	-4.21 ± 3.2
5	10^{-13}	1.34 ± 0.10	-0.77 ± 0.13	-3.67 ± 3.1
0.5	10^{-12}	1.36 ± 0.12	-0.76 ± 0.16	-3.94 ± 3.4
5	10^{-12}	1.27 ± 0.10	-0.64 ± 0.12	-1.75 ± 2.8

is indeed real. Here, we will just present some further tests for our sample.

The fundamental plane is an extension of radio/X-ray correlations in XRBs (Gallo et al. 2003). This correlation is highly significant and is not effected by distance effects as we can trace individual objects on the correlation. In AGN, Hardcastle & Worrall (1999) and Canosa et al. (1999) showed that a radio/X-ray correlation exists and is also not created as an artifact of plotting "distance against distance" in a flux limited sample. If one combines these two correlations with a mass term (which is needed, see Falcke & Biermann 1996), one arrives naturally at the fundamental plane.

One method to check if a correlation between two observables is only created by a third variable, is the partial correlation coefficient. In our case for radio and X-ray luminosity is the parameter that may create a spurious correlation the distance. The correlation coefficient is defined as:

$$r_{rx,d} = \frac{r_{rx} - r_{rd}r_{xd}}{\sqrt{(1. - r_{xd}^2)(1. - r_{rd}^2)}},$$ (9)

where r_{ab} is the normal Pearson R for a and b. This correlation coefficient should remove the effect of the different distances.

If we fix the mass coefficient $\xi_M = -0.85$, we find $r_{rx,d} = 0.91$. We have written a small Monte Carlo simulation, to test if this coefficient is significant. We assume a uniform distribution for the distances and the fluxes in log-space, and assume that the fluxes are uncorrelated. We created 10^6 artificial datasets, and found that not a single dataset had a partial correlation coefficient as large as 0.8, even though the average normal correlation coefficient for the luminosities was 0.99. The standard deviation of the partial correlation coefficient is 0.11 and the mean, 0. Thus, the radio/X-ray correlation with a fixed mass coefficient is significant at the 8σ level. However, in our sample, we only include objects with measured radio and X-ray fluxes and do not include upper limits which could affect the significance.

On the other hand, if we fix $\xi_M = 1.4$ the fundamental plane suggests that $\frac{L_X}{L_R^{1.4}}$ and M are correlated. The Kendall τ for this correlation is $\tau = 0.6$, which is significant as for uncorrelated data τ is normally distributed around 0 with a standard deviation of 0.006. Again we can check whether this is due to the different distances in the sample: The partial correlation coefficient is $r_{L_X/L_R^{1.4},M,D} = 0.84$, which is again significant (7σ).

Even if the observational flux limits can not create a spurious fundamental plane, these limits might still bias the estimated parameters. This problem can be tested with our Monte Carlo simulation. We start with our fundamental plane and observe the parameter changes due to increasing flux limits. As the flux limits may reduce the observed scatter around the fundamental plane, we increase the intrinsic scatter by a factor of 2. The results are summarized in Table 3. As long as the flux limits stay in a reasonable range, the changes to the parameters are below 0.1, i.e., they are of the order of the uncertainties of the fits.

3.2. Comparison of the KFC sample and the MHDM sample

The correlation coefficient ξ_R in the MHDM sample and its subsamples seems larger than those usually found in the KFC sample and a similar effect can be found for ξ_M. The fits of the KFC sample and its subsamples are in agreement with the value found for LH state XRBs ($\xi_R = 1.4$), while the deviations are larger for the MHDM sample. This may be seen as a hint that the MHDM sample is not simply a continuation of the LH state correlation for XRBs, but it may contain other effects like a different source of emission.

The main statistical difference between the MHDM sample and the KFC sample is the smaller intrinsic scatter of the latter: $\sigma_{int} = 0.39$ compared to $\sigma_{int} = 0.65$. It is hard to assess the uncertainties of this value due to selection effects as the underlying distribution is unknown. Bootstrapping yields an error for both values around 0.06.

The discrepancy is partly due to the fact that the KFC sample has less AGN compared to XRBs than the MHDM sample. However, even if one adds the Seyferts and transition objects of Nagar et al. (2005) to create a sample of similar size than the MHDM sample, then the intrinsic scatter is still less ($\sigma_{int} = 0.46$) than for the MHDM case. The same is true for the subsamples of similar size.

The most homogeneous subsample is the sample containing only LLAGN, LH state XRBs and Sgr A*. Here we find $\sigma_{int} = 0.11$. This low value is not only due to the fact that we overestimated the errors of the XRBs, as the numerical value is below 0.1 for the LLAGN sample without XRBs as well. Thus, the correlation is extremely tight for the lowest luminosity objects. If we extend this sample to slightly higher accretion rates, i.e., include FR-I RGs and BL Lac objects the scatter increases due to peculiarities of these objects. The scatter further increases if we included objects FKM classify as high state objects. Thus, the reduced scatter supports the classification of AGN classes by FKM and suggests that there is a difference between LH state AGN and HS state objects.

3.3. Interpretation in the context of the proposed models

In Fig. 4, we show the $\hat{\chi}^2$ maps of the different samples and the predictions of the jet model and one disk/jet model. For the "jet only" model the predicted values are: $\xi_R = 1.38$ and $\xi_M = -0.81$ (FKM) while the values for the "ADAF/jet" model are $\xi_R = 1.64$ and $\xi_M = -1.3$ (MHDM). The exact value for a disk/jet model depends on the solution used for the accretion flow.

The full KFC sample contains some sources, for which we used optical fluxes to derive our equivalent X-ray luminosities. Thus, the "ADAF/jet" does not have to be valid. If we ignore this, the full KFC sample seems to favour the "jet only" model as, according to the confidence region, we can rule out the "ADAF/jet" possibility by more than 3σ. *However*, the exact fit values

depend on the choice of the sample and the used assumptions for the statistical model.

In contrast to the claims of Heinz (2004), the correlation *is* in agreement with a simple jet model in the regime where radiative cooling is not important. The choice of sources minimizes the effect of radiative cooling and the synchrotron cut-off as discussed in Sect. 2.5, but it can not be ruled out that cooling has some effect on this sample.

The correlation with the least scatter is found for the subsample of the KFC sample containing only LH state XRBs, Sgr A* and LLAGN. Its confidence region is shown in the middle row of the figure. As this subsample consists of "real" radio/X-ray data, both models claim to be valid. However, the fit is not in good agreement with both models. The "jet only" model is disfavoured with $\approx 3\sigma$ while the "ADAF/jet" model is even stronger rejected. The remarkable low scatter in this subsample $\sigma_{\rm Int} = 0.10$ supports the idea that LH state XRBs and LLAGN are indeed associated.

In the light of the jet model, it may be that the deviation of the fit from the predicted value is due to synchrotron cooling and the synchrotron cut-off. Even though we have designed this sample to minimize their effect, it may still play a role in some of the objects. To analyze this effect, one would have to compare the X-ray spectrum with the assumed hard power-law and take the spectral index into account. If one finds significant deviations in the spectral index one will have to resort to a more complicated study where the measured spectral index or a more complicated model of the SED is taken into account in the fitting. Another possible explanation for this deviation, is that we do not treat the coupled errors of the XRB data points correctly. As we treat all errors as independent we do not constrain the correlation index $\xi_{\rm R}$ from the XRBs as well as we could. If we set this index to $\xi_{\rm R} = 1.4$ and only fit $\xi_{\rm M}$ we find $\xi_{\rm M} = -0.85$ for the KFC subsample containing LLAGN and XRBs. See also Fig. 5. This is roughly in agreement with the value predicted by the jet/synchrotron model of $\xi_{\rm M} = -0.81$.

For a "disk/jet" model the discrepancy may be due to the disk model used. Besides the discussed ADAF solution, one can use any other accretion flow model to create the X-rays. This can change the prediction considerably, see e.g., MHDM. Thus, the discrepancy of the fit compared to the model predictions can not rule out any of the suggested models with certainty, but – in contrast to earlier claims – it does not support them either.

To compare the edited MHDM sample with the models, we now have to note that the "jet only" model claims to become invalid for the X-ray emission of high state objects like Quasars. Interestingly, the edited MHDM sample including high-state objects indeed disfavours the "jet only" model and is in agreement with the "ADAF/jet" model (1.2σ). However, also for this sample the selection effects are dominating the exact fit value as well.

3.4. The conspiracy

We have seen that the fundamental plane in the two described incarnations is only slightly different. For both samples we find only slightly different parameters, and the scatter seems to be less in the case of the KFC sample. The MHDM sample contains low luminosity objects as well as bright quasars. However, there do not seem to be obvious outliers.

The radio emission is usually attributed to the jet. For the higher observation frequencies there are objects in the two samples that are clearly jet dominated and others for which the accretion flow will be the dominant part at higher frequencies. The clearest examples for synchrotron emission are the BL Lac

objects in the KFC sample but, also for FR-I RG this origin is well established (Chiaberge et al. 1999). On the other hand, the X-ray emission from radio quiet Quasars is very likely not synchrotron emission. Nevertheless, even though the inclusion of the Quasar subsample changes the correlation and increases the scatter, they do not drop off the correlation like HS state XRBs. Likewise, if the X-rays of LH state XRBs and LLAGN are created by the accretion flow, why do the BL Lac objects and FR-I RGs still follow the fundamental plane? There seem to be a "fundamental plane conspiracy": even though the emission processes are different the objects all lie near the fundamental plane.

Within the jet model one can explain part of the conspiracy by the different emission processes (see Fig. 2). If we observe a source at a frequency after the synchrotron cut-off, the Compton branch takes over. The inverse Compton emission can in many sources reach the values one would find if one extrapolates the synchrotron power-law to X-ray frequencies. It will mainly increase the scatter in the correlation.

4. Conclusions

In the previous sections we have reconfirmed the existence of the fundamental plane of accreting black hole in the black hole mass, radio and X-ray luminosity space. We find that the result of a statistical analysis of the radio/X-ray correlation depends strongly on the assumptions of the distribution and magnitude of the measurement errors and the intrinsic scatter. The measurement uncertainties have been taken from the literature. The unknown intrinsic scatter, e.g., the scatter due to relativistic beaming, non-simultaneous observations or source peculiarities, has been parameterized and estimated for the observed samples.

Using this refined method we compared the proposed radio/X-ray correlations of MHDM and the improved KFC sample based on FKM. Both samples differ in their source selection: while the KFC sample tries to include only sources belonging to the low/hard state, the MHDM sample includes all kinds of AGN. Also the observing frequencies differ for some sources, as the KFC sample uses extrapolated optical fluxes for FR-I RGs and BL Lac objects.

The best fit values of both samples depend on the relative number of sources in each class of objects, e.g., the relative number of quasars or FR-I RGs compared to LLAGN. This can be understood if different physical processes are dominant in the different classes, e.g., the emission from LLAGN may be due to the jet, while for quasars the disk emission dominates. The confidence regions do not reflect this problem and have to be viewed as a lower bound on the errors of the parameters.

The best fit values found for the KFC sample are $\xi_{\rm R} = 1.41 \pm 0.11$ and $\xi_{\rm M} = -0.87 \pm 0.14$ while we find for the MHDM sample $\xi_{\rm R} = 1.74 \pm 0.20$ and $\xi_{\rm M} = -1.35 \pm 0.27$. Thus, the KFC sample suggests a simple uncooled "jet only" model while the MHDM sample favours the "ADAF/jet" model. However, the selection effects are very hard to control.

The KFC sample seems to be a more homogeneous sample, as it has a lower intrinsic scatter. The fundamental plane for the subsample containing only LLAGNs and XRBs is surprisingly tight with a scatter of $\sigma_{\rm int} = 0.12$ dex, while the full sample has $\sigma_{\rm int} = 0.38$. Compared to this, the MHDM sample has a higher intrinsic scatter of $\sigma_{\rm int} \approx 0.6$ dex. This supports the AGN classification of FKM in low/hard and high/soft state objects.

In general, the fundamental plane of black hole activity is confirmed by our analysis. With a careful control of a homogeneous source selection (high-state versus low-state), the scatter can reach rather low values. This promises a wider application

of the "fundamental plane" in other contexts (see e.g., Merloni 2004; Maccarone 2005) and calls for improved radio and X-ray surveys in the future.

References

Abramowicz, M. A., Kluźniak, W., McClintock, J. E., & Remillard, R. A. 2004, ApJ, 609, L63
Antonucci, R. 1993, ARA&A, 31, 473
Baganoff, F. K., Bautz, M. W., Brandt, W. N., et al. 2001, Nature, 413, 45
Baganoff, F. K., Maeda, Y., Morris, M., et al. 2003, ApJ, 591, 891
Barcons, X., Carrera, F. J., Watson, M. G., et al. 2002, A&A, 382, 522
Bettoni, D., Falomo, R., Fasano, G., et al. 2001, A&A, 380, 471
Blandford, R. D., & Rees, M. J. 1978, in Proc. of the Pittsburgh Conference on BL Lac Objects, 1978, 328
Canosa, C. M., Worrall, D. M., Hardcastle, M. J., & Birkinshaw, M. 1999, MNRAS, 310, 30
Chiaberge, M., Capetti, A., & Celotti, A. 1999, A&A, 349, 77
Chiaberge, M., Celotti, A., Capetti, A., & Ghisellini, G. 2000, A&A, 358, 104
Corbel, S., Fender, R. P., Tzioumis, A. K., et al. 2000, A&A, 359, 251
Corbel, S., Nowak, M. A., Fender, R. P., Tzioumis, A. K., & Markoff, S. 2003, A&A, 400, 1007
D'Agostini, G. 2005 [arXiv:physics/0511182]
Esin, A. A., McClintock, J. E., & Narayan, R. 1997, ApJ, 489, 865
Falcke, H., & Biermann, P. L. 1995, A&A, 293, 665
Falcke, H., & Biermann, P. L. 1996, A&A, 308, 321
Falcke, H., & Biermann, P. L. 1999, A&A, 342, 49
Falcke, H., Malkan, M. A., & Biermann, P. L. 1995, A&A, 298, 375
Falcke, H., Körding, E., & Markoff, S. 2004, A&A, 414, 895
Fanaroff, B. L., & Riley, J. M. 1974, MNRAS, 167, 31P
Fender, R., Corbel, S., Tzioumis, T., et al. 1999, ApJ, 519, L165
Fender, R. P. 2001, MNRAS, 322, 31
Fender, R. P., Gallo, E., & Jonker, P. G. 2003, MNRAS, 343, L99
Ferrarese, L., & Ford, H. 2005, Space Sci. Rev., 116, 523
Fossati, G., Maraschi, L., Celotti, A., Comastri, A., & Ghisellini, G. 1998, MNRAS, 299, 433
Gallo, E., Fender, R. P., & Pooley, G. G. 2003, MNRAS, 344, 60
Ghisellini, G., Celotti, A., & Costamante, L. 2002, A&A, 386, 833
Haardt, F., & Maraschi, L. 1991, ApJ, 380, L51
Hardcastle, M. J., & Worrall, D. M. 1999, MNRAS, 309, 969
Harris, D. E., & Krawczynski, H. 2002, ApJ, 565, 244
Hawkins, E., Maddox, S., Cole, S., et al. 2003, MNRAS, 346, 78
Heinz, S. 2004, MNRAS, 355, 835
Heinz, S., & Merloni, A. 2004, MNRAS, 355, L1
Homan, J., Buxton, M., Markoff, S., et al. 2005, ApJ, 624, 295
Hynes, R. I., Steeghs, D., Casares, J., Charles, P. A., & O'Brien, K. 2003, ApJ, 583, L95
Hynes, R. I., Steeghs, D., Casares, J., Charles, P. A., & O'Brien, K. 2004, ApJ, 609, 317
Jonker, P. G., & Nelemans, G. 2004, MNRAS, 354, 355

Kellermann, K. I., Sramek, R., Schmidt, M., Shaffer, D. B., & Green, R. 1989, AJ, 98, 1195
Körding, E., & Falcke, H. 2004, A&A, 414, 795
Maccarone, T. J. 2005, MNRAS, 360, L30
Maccarone, T. J., Gallo, E., & Fender, R. 2003, MNRAS, 345, L19
Maoz, D., Nagar, N. M., Falcke, H., & Wilson, A. S. 2005, ApJ, 625, 699
Markoff, S. 2005, ApJ, 618, L103
Markoff, S., Falcke, H., & Fender, R. 2001a, A&A, 372, L25
Markoff, S., Falcke, H., Yuan, F., & Biermann, P. L. 2001b, A&A, 379, L13
Markoff, S., Nowak, M., Corbel, S., Fender, R., & Falcke, H. 2003, A&A, 397, 645
Markoff, S., & Nowak, M. A. 2004, ApJ, 609, 972
Markoff, S., Nowak, M. A., & Wilms, J. 2005, ApJ, 635, 1203
Markowitz, A., Edelson, R., Vaughan, S., et al. 2003, ApJ, 593, 96
Marshall, H. L., Harris, D. E., Grimes, J. P., et al. 2001, ApJ, 549, L167
Marshall, H. L., Schwartz, D. A., Lovell, J. E. J., et al. 2005, ApJS, 156, 13
McClintock, J., & Remillard, R. 2006, in Compact Stellar X-ray Sources, ed. W. H. G. Lewin, & M. van der Klis (Cambridge University Press)
Merloni, A. 2004, MNRAS, 353, 1035
Merloni, A., Heinz, S., & Di Matteo, T. 2003, MNRAS, 345, 1057
Merloni, A., Koerding, E., Heinz, S., et al. 2006 [arXiv:astro-ph/0601286]
Merritt, D., & Ferrarese, L. 2001, ApJ, 547, 140
Mirabel, I. F., & Rodríguez, L. F. 1999, ARA&A, 37, 409
Nagar, N. M., Falcke, H., & Wilson, A. S. 2005, A&A, 435, 521
Narayan, R., & Yi, I. 1994, ApJ, 428, L13
Nowak, M. A., Wilms, J., Heinz, S., et al. 2005, ApJ, 626, 1006
Orosz, J. A. 2003, in IAU Symp., 365
Piconcelli, E., Jimenez-Bailón, E., Guainazzi, M., et al. 2005, A&A, 432, 15
Poutanen, J. 1998, in Theory of Black Hole Accretion Disks (Cambridge University Press), 100
Press, W. H. 2002, Numerical recipes in C++ : the art of scientific computing by William H. Press. xxviii, 1,002 p. : ill.
Prugniel, P., Zasov, A., Busarello, G., & Simien, F. 1998, A&AS, 127, 117
Ptak, A., & Griffiths, R. 2003, in Astronomical Data Analysis Software and Systems XII, ASP Conf. Ser., 295, 465
Quataert, E., & Gruzinov, A. 2000, ApJ, 539, 809
Reeves, J. N., & Turner, M. J. L. 2000, MNRAS, 316, 234
Reig, P., Belloni, T., & van der Klis, M. 2003, A&A, 412, 229
Ribó, M., Combi, J. A., & Mirabel, I. F. 2005, Ap&SS, 297, 143
ROSAT Scientific Team 2000, VizieR Online Data Catalog, 9028, 0
Sambruna, R. M., Gambill, J. K., Maraschi, L., et al. 2004, ApJ, 608, 698
Shahbaz, T., Fender, R., & Charles, P. A. 2001, A&A, 376, L17
Shakura, N. I., & Sunyaev, R. A. 1973, A&A, 24, 337
Spergel, D. N., Verde, L., Peiris, H. V., et al. 2003, ApJS, 148, 175
Stirling, A. M., Spencer, R. E., de la Force, C. J., et al. 2001, MNRAS, 327, 1273
Sunyaev, R. A., & Trümper, J. 1979, Nature, 279, 506
Tananbaum, H., Gursky, H., Kellogg, E., Giacconi, R., & Jones, C. 1972, ApJ, 177, L5
Tavecchio, F., Maraschi, L., Ghisellini, G., et al. 2002, ApJ, 575, 137
Terashima, Y., & Wilson, A. S. 2003, ApJ, 583, 145
Thorne, K. S., & Price, R. H. 1975, ApJ, 195, L101
Tonry, J. L., Dressler, A., Blakeslee, J. P., et al. 2001, ApJ, 546, 681
Trussoni, E., Capetti, A., Celotti, A., Chiaberge, M., & Feretti, L. 2003, A&A, 403, 889
Tully, R. B. 1988, Nearby galaxies catalog (Cambridge and New York: Cambridge University Press), 221
Uttley, P., McHardy, I. M., & Papadakis, I. E. 2002, MNRAS, 332, 231
Woo, J., & Urry, C. M. 2002, ApJ, 579, 530
Young, A. J., & Wilson, A. S. 2004, ApJ, 601, 133